GEOPHYSICS, VOL. 87, NO. 2 (MARCH-APRIL 2022); P. T99–T109, 12 FIGS.
10.1190/GEO2020-0874.1

Impacts of model resolution on multiple prediction

Yue Ma[1], Yujin Liu[1], and Yi Luo[2]

ABSTRACT

Despite theoretical advancements in multiple identification and elimination, the application and success of these advancements are questionable in some cases and are limited to marine environments, especially deepwater. In land seismic, however, a clear understanding of the internal multiple generators is not readily available; thus, efforts to attenuate them often are quite ineffective. We have analyzed, in the case of many thin layers, how the primaries and multiples are affected by fine-scale variations in the velocity model. Cross-coherence is used to measure the similarity of the original primaries/multiples and the ones generated from upscaled velocity models. The combined use of kurtosis and the cross-coherence method enables us to precisely quantify the impact of fine layering on multiples. Test results demonstrate that surface-related multiples and internal multiples are much more sensitive than the primaries to thickness variations of the velocity model. As the thickness of each upscaled layer varies from 1 to 21 m, multiples change rapidly, whereas primaries are almost the same. The high sensitivity of internal multiples on fine layering suggests that the detailed model information should be considered in model parameterization in the internal multiple removal, especially for model-driven methods.

INTRODUCTION

Primaries and multiples contain subsurface information relevant to the location and production of hydrocarbons. However, unraveling structural and stratigraphic information from multiples is still a difficult task. Back-propagating a wavefield containing primaries and multiples for migration imaging and inversion is usually beyond our ability to provide a satisfying image. Especially for a smooth and continuous migration velocity model (generally assumed in practice), multiples will result in a false, misleading, and potentially injurious subsurface image (Weglein, 2016). Therefore, primaries are typically considered as signal, and multiples are usually considered a form of coherent noise to be removed prior to extracting subsurface information.

Estimation and attenuation of multiples, especially onshore internal multiples, from seismic data remains one of the biggest challenges in exploration seismology. Surface-related multiple elimination (Berkhout and Verschuur, 1997) has emerged as a key methodology applicable for marine seismic data sets, especially in deepwater. In land seismic data sets, a huge effort has been made to remove internal multiples over the years. Radon-based methods are commonly used for multiple attenuation in land seismic data processing, assuming a velocity discrimination between primaries and multiples (Trad et al., 2003). Berkhout and Verschuur (2005) use principles from the common focal point (CFP) technology and develop a data-driven method in which all internal multiples generated within a specific layer or by a boundary are taken into account. In this method, the kinematics of internal multiples are obtained as convolution of the semiredatumed CFP gathers (source at the surface and receivers at the reflecting interface). An adaptive subtraction is then commonly used to estimate the dynamics (i.e., amplitude) of the multiples. Kelamis et al. (2002) and Luo et al. (2007) demonstrate this method on land data and develop a series of practical methodologies in the shot, common-midpoint, and stack domain for internal multiple attenuation. In these schemes, prior knowledge of the main multiple generators is required. Unlike surface-related multiples with only one clear reflecting boundary at the surface that almost reflects all energy into the subsurface, every millimeter of earth is a possible downward scatterer to generate internal multiples. Thus, the application of the CFP-based technology is not always straightforward because it requires the definition of several discrete multiple generators.

Another method of internal multiple attenuation, pioneered by Araújo et al. (1994) and Weglein et al. (1997), uses the inverse scattering series (ISS) to predict internal multiples for all horizons at

Manuscript received by the Editor 1 December 2020; revised manuscript received 23 September 2021; published ahead of production 10 November 2021; published online 10 January 2022.
[1]Aramco Beijing Research Center, Aramco Asia, Beijing 100102, China. E-mail: yue.ma@aramcoasia.com; yujin.liu@aramcoasia.com (corresponding author).
[2]Saudi Aramco, EXPEC Advanced Research Center, Dhahran 31311, Saudi Arabia. E-mail: yi.luo@aramco.com.

DOI:10.1190/geo2020-0874.1

once. This method is fully data-driven and does not require any information about the multiple generators or the medium through which the multiples propagate. Depending on the implementation complexity, it is possible to predict either an approximation of the first-order internal multiples or the infinite series of internal multiple contributions with the correct traveltime and better estimate of the amplitudes (Ramirez and Weglein, 2008). Matson et al. (1999) are the first to apply the ISS internal multiple attenuation algorithm to marine data. This method has been demonstrated on land data by Fu et al. (2010). All of the aforementioned methods rely on some form of adaptive subtraction to effectively eliminate internal multiples. Adaptive subtraction runs into problems when the predicted internal multiples are proximal to or interfering with primaries over relatively large-offset ranges (Abma et al., 2002). To reduce the subtraction leakage, a closed-loop implementation has been proposed by van Groenestijn amd Verschuur (2009) for estimation of primaries by sparse inversion (EPSI) for the surface-multiple case. Ypma and Verschuur (2013) generalize the EPSI method to remove surface and internal multiples. It shows better results in retaining the primary amplitudes, but it is rather computationally intensive and requires some prior knowledge about the subsurface.

Recently, a series of data-driven methods have emerged for internal multiple removals. Löer et al. (2016) propose an ISS-based internal multiple attenuation scheme that can be used to predict all orders of internal multiple reflections with approximate amplitudes in one step without model information. Van der Neut and Wapenaar (2016) propose a Marchenko multiple elimination (MME) scheme to remove internal multiple reflections from the measured acoustic reflection response without adaptive subtraction. It is derived from the coupled Marchenko equations and requires smooth model information to create offset-dependent time truncations. The MME scheme has been modified to remove the need for model information by Zhang and Staring (2018), and further to compensate for the transmission losses in primary reflections (Zhang et al., 2019). The transmission compensated MME (T-MME) also has been extended to account for free-surface multiple reflections (Zhang and Slob, 2019). Reinicke et al. (2021) present a representative synthetic case study to analyze the impact of ignoring elastic effects in acoustic Marchenko internal multiple removal method. Elison et al. (2020) present a detailed analysis of the impact of band limitation on the Marchenko methods and propose an augmented Marchenko method with a minimum-phase constraint to account for short-period internal multiples of a horizontally layered overburden. They demonstrate the proposed scheme with a 2D synthetic model based on a sonic log in the Middle East. Another encouraging result from Arabian Gulf shallow-water environments with a complex thin-layered overburden has been published by Staring et al. (2021). They propose a two-step workflow — robust EPSI (Lin and Herrmann, 2013) followed by the double dereverberation Marchenko method — to remove internal multiples without the requirement of any a priori information about the subsurface and adaptive subtractions. A recent study on the impact of elastic effects in acoustic Marchenko demultiple methods shows that converted waves have a substantial influence on the predicted internal multiples. However, the migration image is hardly distorted. Because the Marchenko equation-based approaches require data with true amplitudes, it is crucial that all preprocessing steps are performed in an amplitude-preserving way. In practice, some minor inaccuracies in the processing flow may end up as severe prediction errors for which adaptive subtractions are necessary to obtain the best results. Despite such great advancements havng been made over the years, proper removal of internal multiples is still not fully achievable. A complex near surface combined with poor signal-to-noise ratio and source/receiver coupling issues are key obstacles that deteriorate the performance of multiple attenuation algorithms. Especially in land seismic data sets, a clear understanding of multiples of different orders and their generators is not readily available. As shown by Kelamis et al. (2006), in land, most internal multiples are generated by a variety of complex thin layers encountered in the near surface. Liang et al. (2012) use a reflector spectrum to further verify that internal multiples originated from many reflectors distributed throughout the model, rather than from a few major ones. Therefore, land internal multiples cannot be eliminated by removing the effect of any single reflector or even a few major reflectors. Internal multiple removal methods that assume a few major generators may be challenged. Particularly in desert terrains with a complex near surface and low-relief structures, internal multiples can easily overwhelm the weak target primary reflections because of the presence of alternating high- and low-velocity layers upon the first kilometer, where velocities can go to as high as 5000 m/s followed by a layer of 2500 m/s. This is a typical near-surface karsts geological structure in the Arabian Peninsula. The SEG Advanced Modeling (SEAM) Arid model (Oristaglio, 2013) features such extreme velocity contrast in a 500 m near surface that juxtaposes hard carbonate bedrock and soft unconsolidated sediments. These strong velocity inversions in the near surface reduce the effectiveness of most of the moveout-based methods, create major problems in velocity analysis (Shen et al., 2012), and result in a strong leakage of multiple energy in the migration image (Luo et al., 2011; Verschuur and Berkhout, 2015).

Thick layers, which often represent geological epochs, may have interfaces with large reflection coefficients. In such situations, reflections are isolated and multiples are considered as noise; we may have a chance of predicting and removing internal multiples. However, in reality, we have layers with all kinds of thicknesses and contrasts. It is well known that the short-period internal multiples in a series of thin layers have the effect of delaying, shaping, and magnifying the transmitted energy through those layers, and may surpass its amplitude (see the effective medium theory in O'Doherty and Anstey, 1971). The transmission effects also were mentioned by Verschuur and Berkhout (2015). They use a thin-layer model to demonstrate that internal multiple removal will become a huge challenge because transmission effects make the true primary much smaller in amplitude than multiples.

The goal of this work is to show, in the case of many thin layers, how the primaries and multiples are affected by the fine-scale variations in the velocity model. We first generate a series of primaries and multiples of infinite orders by reflectivity forward modeling based on a sonic log for different upscaling scales. Then, we apply the cross-coherence method, which calculates the crosscorrelation of traces normalized by their spectral amplitudes in the frequency domain, to measure the time alignment of the synthesized traces. This cross-coherence method effectively removes the amplitude information, revealing the frequency-independent phase changes between two traces. We quantify the impact of fine layering on primaries and multiples by measuring the kurtosis of the cross-coherence results. Test results demonstrate that surface-related multiples and internal multiples are much more sensitive to the fine-scale variations in the velocity model than the primaries. They

exhibit rapid changes when the velocity model upscales slightly, whereas the primaries are completely unchanged. In such circumstances, the high sensitivity of internal multiples on fine layering suggests that the detailed model information should be considered in model parameterization in the internal multiple removal, especially for model-driven methods.

METHOD

The method developed in this paper is based on the reflectivity forward-modeling method, which constructs the reflection response in a two-stage recursive process for incident downgoing waves (Kennett, 2003). The seismogram is the result of the convolution of the source function with the obtained reflectivity response function. The reflectivity method is able to model the cumulative effect of a sequence of internal reverberations. Primaries and internal multiples can be separated by truncating the expansions of the reverberation operator in the forward modeling (see Appendix A for details).

Cross-coherence

Crosscorrelation is widely used to measure the similarity of two traces u_a and u_b:

$$C_{ab} = u_a^* u_b, \tag{1}$$

where the asterisk denotes a complex conjugate. We use a frequency-domain formulation for all analysis and the dependence on frequency is suppressed in the notation. The cross-coherence defined in the frequency domain is

$$H_{ab} = \frac{u_a^* u_b}{|u_a||u_b|}. \tag{2}$$

The numerator of equation 2 is the same to the right side in the crosscorrelation, and the denominator is the product of the amplitude spectra of the traces. The cross-coherence function indicates that, although the phase of each trace is used, the amplitude information is ignored. Because the amplitude is prone to being inaccurate in practice, the use of this cross-coherence function is expected to retrieve more robust phase information than crosscorrelation. This method is used in seismology by Aki (1957) at first, and then widely applied in seismic interferometry due to its extraordinary capability in suppressing the influence of additive noise and amplitude variations among the input traces (Bensen et al., 2007; Nakata et al., 2011; Liu et al., 2020b).

The crosscorrelation function and the cross-coherence function have the characteristic that, if the two traces are identical in shape, but shifted in time, the maximum correlation/coherence occurs at the time lag at which they are most similar; however, if the two traces are totally different, the correlation/coherence results in the time domain tend to be random distributions. Note that the maximum correlation occurs at zero lag in the autocorrelation result. However, there is only a single spike at zero lag in the autocoherence in the limit of an infinitely long sequence.

We analyze the sensitivity of the crosscorrelation and the cross-coherence functions on measuring the time alignment of two traces. Assume that u_a is the trace modeled with the original thin-layer velocity model and u_b is generated with a slightly upscaled velocity model. Then, u_b can be seen as a combination of u_a and an error term m, that is, $u_b = u_a + m$. Based on the Rayleigh's limit of resolution, the vertical seismic resolution generally is one quarter of the dominant wavelength. Reflectors that closely situated within 1/4 wavelength cannot be resolved on seismic reflections (i.e., primaries). However, the short-period internal multiples that reverberate within thin layers have longer and more complicated traveling paths. Therefore, internal multiples are more sensitive to the velocity model changes than the primaries. If the thickness of each layer of the velocity model changes within 1/4 wavelength, the primaries of u_a and u_b remain the same. The error term m comes from the difference of internal multiples between u_a and u_b. The crosscorrelation of u_a and u_b is

$$C_{ab} = u_a^*(u_a + m) = u_a^* u_a + u_a^* m. \tag{3}$$

It consists of an autocorrelation of u_a and a crosscorrelation of u_a and the error term m. The influence of the model upscaling, that is, the error term m, in the crosscorrelation result appears in the second term $u_a^* m$ only.

The cross-coherence function of the two traces u_a and u_b is

$$H_b = \frac{u_a^*(u_a + m)}{|u_a||u_a + m|} \tag{4}$$

$$= \frac{u_a^*}{|u_a|}\frac{u_a + m}{\sqrt{(u_a^* + m^*)(u_a + m)}} \tag{5}$$

$$= \frac{u_a^*}{|u_a|^2}\frac{u_a + m}{\sqrt{1 + \frac{u_a^* m + m^* u_a + |m|^2}{|u_a|^2}}}. \tag{6}$$

Assuming that the energy of the error term $|m|$ is smaller than the energy of the trace $|u_a|$, that is, $|m|/|u_a| < 1$, equation 6 can be expanded as

$$H_{ab} = \frac{u_a^*(u_a + m)}{|u_a|^2}\left(1 + \sum_{n=1}^{\infty}\frac{\prod_{k=1}^{n}\left(\frac{1}{2} - k\right)}{n!}\left(\frac{u_a^* m + m^* u_a + |m|^2}{|u_a|^2}\right)^n\right). \tag{7}$$

Ignoring the terms higher than the second order, we obtain

$$\begin{aligned} H_{ab} &= \frac{u_a^*(u_a + m)}{|u_a|^2}\left(1 - \frac{1}{2}\frac{u_a^* m + m^* u_a + |m|^2}{|u_a|^2} + \frac{3(u_a^* m + m^* u_a + |m|^2)^*(u_a^* m + m^* u_a + |m|^2)}{8|u_a|^4}\right) \\ &= \frac{u_a^*(u_a + m)}{|u_a|^2}\left(1 - \frac{1}{2}\frac{u_a^* m + m^* u_a + |m|^2}{|u_a|^2} + \frac{3mu_a^* u_a^* m + u_a m^* m^* u_a + 2u_a m^* u_a^* m}{8|u_a|^4}\right) \\ &= \left(1 - \frac{1}{4}\frac{|m|^2}{|u_a|^2}\right)\frac{u_a^* u_a}{|u_a|^2} + \frac{1}{2}\frac{u_a^* m - m^* u_a}{|u_a|^2} + \frac{1}{8}\frac{3u_a m^* m^* u_a - mu_a^* u_a^* m}{|u_a|^4}. \end{aligned} \tag{8}$$

Note that the noise term m arisen from the model upscaling contributes to each term. Therefore, the cross-coherence function is strongly influenced by the fine layering in the velocity model, compared with the crosscorrelation in equation 3.

Figure 1 demonstrates the sensitivity of the crosscorrelation and cross-coherence functions on measuring the time alignment of two simple traces. Figure 1a and 1b shows two simulations of the impulse

responses. The event at 2 s is the only difference between the two traces. Figure 1c gives the crosscorrelation result of traces in Figure 1a and 1b. Figure 1d and 1e corresponds to the first and second term of equation 3, respectively. Note that Figure 1d is actually the autocorrelation of the trace shown in Figure 1a, and Figure 1e reveals the difference between the traces in Figure 1a and 1b. The cross-coherence result is shown in Figure 1f with its leading-order term (the first term in equation 8) shown in Figure 1g and the higher order terms (the second and third term in equation 8) shown in Figure 1h. Compared with the corresponding crosscorrelation result in Figure 1c–1e, the difference between the two traces has a profound influence on each term in the cross-coherence result. Moreover, we observe that the cross-coherence result (Figure 1f) exhibits a spikier pattern than the crosscorrelation result (Figure 1c).

Kurtosis

To investigate the influence of fine-scale variations of the velocity model on primaries and internal multiples, we need an appropriate tool to analyze the sensitivity of the crosscorrelation and the cross-coherence functions on measuring how much two traces resemble each other. The kurtosis of a time series $\{x_i\}_{i=1}^{N}$ is defined as

$$K(x) = \frac{\frac{1}{N}\sum_{i=1}^{N}(x_i - \bar{x})^4}{s^4}, \tag{9}$$

where $\bar{x}$ is the mean, s is the standard deviation, and N is the number of samples. A similar function was used by Levy and Oldenburg (1987) for the estimation of phase directly from data. It is a statistical measure of the spikiness of a distribution, that is, whether the data are heavy-tailed or light-tailed. The data sets with high kurtosis tend to have heavy tails, or outliers. This occurs when the crosscorrelation/cross-coherence results have a few large spikes, which indicates that the two traces are very much alike in shape. On the other hand, data sets with low kurtosis tend to have light tails or lack of outliers. In our case, low kurtosis of the crosscorrelation/cross-coherence indicates that two traces are not related. The kurtosis of a random Gaussian distribution is three. Kurtosis attains a minimum when the time series consists of equal amplitude elements with no tails.

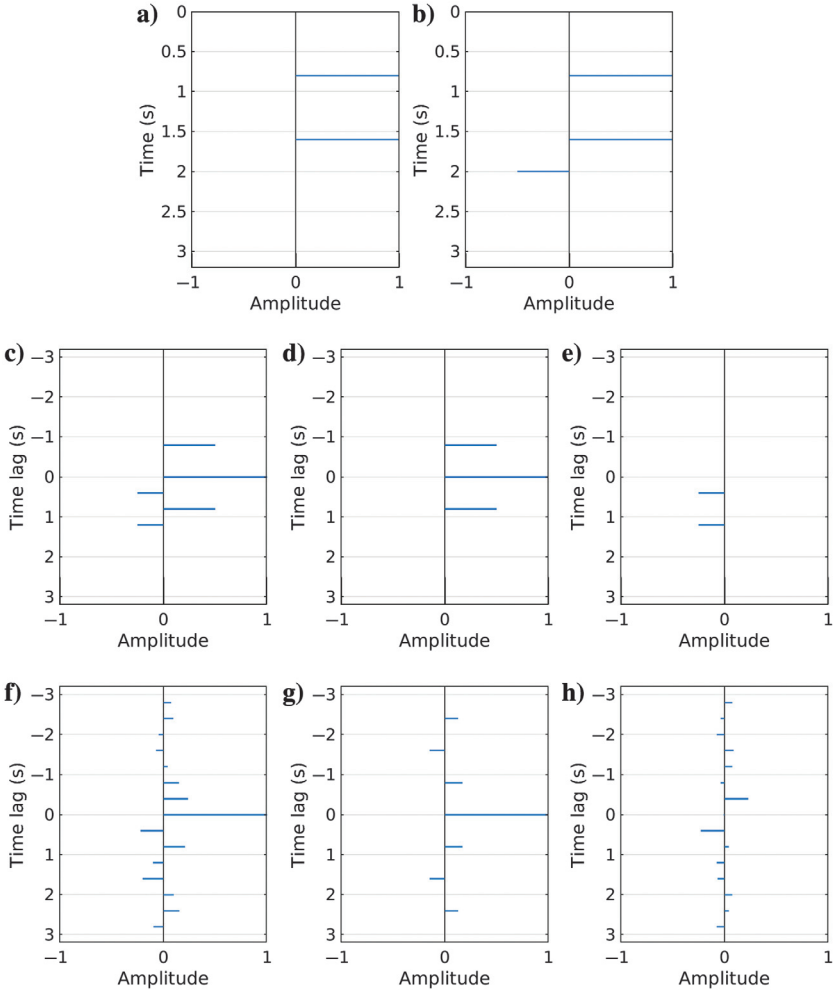

Figure 1. (a and b) Two simulations of the impulse responses. The event at 2 s is the only difference between the two traces. (c) The crosscorrelation result of traces in (a and b). (d and e) The first and second term in equation 3, respectively. The cross-coherence result is shown in (f) with its leading-order term (the first term in equation 8) shown in (g) and the higher order terms (the second and third term in equation 8) shown in (h).

Recall that Figure 1c and 1f is the crosscorrelation and cross-coherence results of the two impulse responses in Figure 1a and 1b, respectively. The kurtosis of the cross-coherence result (Figure 1f) is much larger than the kurtosis of the crosscorrelation result (Figure 1c). It is consistent with the previous observation that, compared with the crosscorrelation (Figure 1c), the cross-coherence function is more sensitive to the slight differences between two traces shown in Figure 1a and 1b. Therefore, the kurtosis can be used as a measurement to quantify the cross-correlation/cross-coherence result, which plays an essential role in analyzing the impact of fine layering on primaries and internal multiples.

SENSITIVITY OF THIN-LAYER INTERNAL MULTIPLES

The reflectivity method is used to generate synthetic traces from a stratified medium (Kennett, 2003). This method is able to model the cumulative effect of a sequence of internal reverberations. Primaries and internal multiples can be separated by truncating the expansions of the reverberation operator in the forward modeling (see Appendix A for details).

Figure 2 illustrates an example using a complex velocity function derived from sonic log (shown in Figure 2a). The number of samples in depth is $nz = 5000$ with sample interval $dz = 1$ m. The log data have a couple of rapid velocity changes between 1243 and 3500 m/s. The alternating high- and low-velocity layers at 2 km depth can be observed on the log, which generates strong short-period internal multiples. The number of samples in time is $nt = 1000$ with time interval $dt = 0.004$ s. A Ricker wavelet with peak frequency of 20 Hz is used in the reflectivity forward modeling. The simulation of

the response with primaries only and all orders of internal multiples only is shown in Figure 2b and 2c, respectively. Figure 2d displays the synthetic trace containing primaries and all orders of internal multiples.

Upscaling of velocity logs, from fine-scale to coarse-scale, is a necessary step in seismic modeling, data processing, and interpretations. In a general sense, upscaling means to replace a heterogeneous volume with a homogeneous volume having effectively equivalent elastic constants. Most of the reliable upscaling methods are based on the effective medium theory that allows one to find an effective stiffness tensor relating the strain and stress fields averaged over a representative volume (Bruggerman, 1937; Backus, 1962). The simplest way for well-log scale data is a calculation of the time-average velocity within a given window. Because the phase velocity is usually not involved in the multiple elimination, as well as the imaging and waveform inversion process, we only consider the velocity upscaling methods with the high-frequency approximation. Comparison of seismic upscaling methods with frequency dependency is referred to Tiwary et al. (2009). Ignoring the density, the time-averaging upscaled velocity v_{TA} is calculated by

$$\frac{1}{v_{\mathrm{TA}}} = \frac{1}{\sum_{i=1}^{N} d_i}\left(\sum_{i=1}^{N} \frac{d_i}{v_i}\right), \tag{10}$$

where N is the length of the window and d_i and $v_i, i = 1, \ldots, N$ are the layer thickness and velocity for the ith layer, respectively. Another frequently used approach for upscaling velocity measurements was proposed by Backus (1962). It allows computation of the long-wavelength effective elastic moduli of a medium composed of a stack of thin, isotropic, and homogeneous layers. The Backus averaging velocity v_{BA} in acoustic media is defined by

$$\frac{1}{v_{\mathrm{BA}}^2} = \frac{1}{\sum_{i=1}^{N} d_i}\left(\sum_{i=1}^{N} \frac{d_i}{v_i^2}\right). \tag{11}$$

Note that because the square terms in the brackets in equation 11 are always positive. The Backus velocity is slower than the time-averaging velocity $v_{\mathrm{BA}} < v_{\mathrm{TA}}$.

In this study, we upscale the sonic log shown in Figure 2a by applying the time-averaging method (equation 10) and Backus averaging method (equation 11) within the depth window of $2, 3, \ldots, 21$ m, respectively. Figure 3a–3e shows a series of selected upscaled blocky velocity models with depth intervals of 1, 6, 11, 16, and 21m, respectively. In each plot, we compare the time-averaging result (the blue curve) with Backus averaging result (the red curve) with the same upscaling window length. As seen in Figure 3, the differences in the upscaling results between the two methods are very small. This is highly consistent with the comparison of seismic upscaling methods conducted by Tiwary et al. (2009), who find that the difference in P-wave velocity gets smaller at higher frequencies than at low frequencies. Here, the frequency independent upscaling equations 10 and 11 used in the test can be seen as a high-frequency limit. Even with the largest window size of 21m, the maximum difference between the two upscaled velocities is only approximately 4%. Then, the upscaled velocity models of the depth interval ranging from 1 to 21 m generated by the two methods are fed into the reflectivity forward-modeling process. We compare the impacts of the two model upscaling methods on the reflection data by one-to-one calculating the cross-coherence of the primaries/internal multiples corresponding to the two upscaled velocity modules. The results are aligned and displayed in Figure 4a and 4b, respectively. Each column in Figure 4a (4b) corresponds to the cross-coherence of primaries (internal multiples) generated by time-averaging and Backus averaging upscaled velocity models with the same depth interval/upscaling window length ranging from 1 to 21 m with an increment of 1 m. As seen in Figure 4a and 4b, there is only one distinct spike-train event at zero-time lag, which indicates that primaries and internal multiples generated by the two different upscaling methods exhibit high similarities in general. As the upscaling window increases, the cross-coherence results of primaries and internal multiples shift upward slightly because the Backus averaging velocity is slower than the time-averaging velocity. Therefore, there is a little time shift on the primary/internal multiples between the two upscaling methods. To better preserve the kinematics of the reflections and avoid duplicate analysis, we use the time-averaging upscaling method in the following tests.

As Rayleigh's limit of resolution states, to resolve for two interfaces that are closely spaced, the wavelength is $\lambda/4$, where λ is the dominant wavelength. If the upscaling window length is smaller than the vertical seismic resolution, which is one quarter of the dominant wavelength, the kinematics of primary reflections will not change. The primaries and internal multiples corresponding to the time-averaging upscaled velocity models of the depth interval ranging from 1 to 21 m with an increment of 1 m are aligned and displayed in Figure 5a and 5b, respectively. As a reference, the first column shows the primaries and internal multiples generated by the original well log. Automatic gain control with 300 ms moving time window was applied on each trace to balance the amplitude difference. In this example, the vertical seismic resolution is approximately 32 m based on the average velocity of 2560 m and the 20 Hz dominant frequency of the wavelet. The upscaling velocity model changes within the vertical seismic resolution. Therefore,

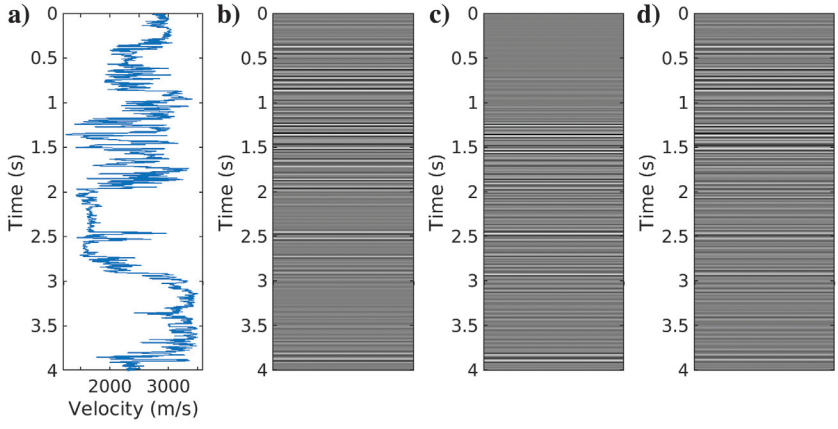

Figure 2. A synthetic example. (a) A sonic log consisting of 5000 layers with 1 m depth interval. (b) The simulation of the response with primaries only. (c) The response with infinite orders of internal multiples only. (d) The response with primaries plus internal multiples.

as we can see in Figure 5a, the influence of fine layering on primaries is almost negligible, especially when the thickness of each layer in the velocity model is less than 15 m. However, short-period internal multiples reverberate several times within a layer. Kinematic differences that are accumulated along the longer and more complicated travel path are visible everywhere throughout the entire internal multiple panel shown in Figure 5b.

To remove the influence of the band-limited wavelet, we also compare the spectra of the impulse response of upscaled primaries (Figure 6a) and internal multiples (Figure 6b), respectively. Each column of the spectra corresponds to an upscaled velocity model of the depth interval ranging from 1 to 21 m with an increment of 1 m. First, we observe that the low-frequency components (<15 Hz) are stable for primaries and internal multiples. As the frequency increases, the influences of the velocity upscaling on the spectra were amplified obviously. Note that, at the dominant frequency of 35 Hz, internal multiples change rapidly with respect to the upscaling window size, whereas the primaries are relatively continuous. Similar phenomena can be observed at almost all the frequency components, which means that internal multiples are much more sensitive than primaries to the fine layering.

We then compute the kurtosis of the cross-coherence functions between the upscaled primaries/multiple and the original ones to quantify the differences. Each column in Figure 7a corresponds to the cross-coherence result between the original primaries and the ones generated with upscaled velocity models. Figure 7b corresponds to the cross-coherence result between the original internal multiples and the ones generated with upscaled velocity models. Figure 7c shows the kurtosis of the primary/multiple cross-coherence results along with the upscaling window size. The overall high kurtosis on the cross-coherence result of primaries (the blue curve in Figure 7c) indicates that the original and upscaled primaries have high similarity. This similarity slightly decreases as the thickness of each layer increases from 11 to 21 m. However, the kurtosis of the cross-coherence result of internal multiples (the red curve in Figure 7c) dramatically drops as the upscaled window increases. Note that changes in the internal multiples can be detected by the kurtosis even when the thickness of each layer changes from 1 to 3 m. Moreover, when the thickness of each layer is larger than 15 m, the kurtosis reaches the level of Gaussian noise (the kurtosis of a random Gaussian distribution is three), which indicates that the upscaled internal multiples and the original scale internal multiples have little similarity.

Figure 8 shows a comparison of the crosscorrelation of the primaries/internal multiples and their kurtosis values. We can see that the resolution of crosscorrelation results of primaries (Figure 8a) and internal multiples (Figure 8b) is much lower than the cross-coherence results (Figure 7a and 7b). Figure 8c shows the kurtosis curves of the crosscorrelation results between the upscaled primaries/multiples and the original

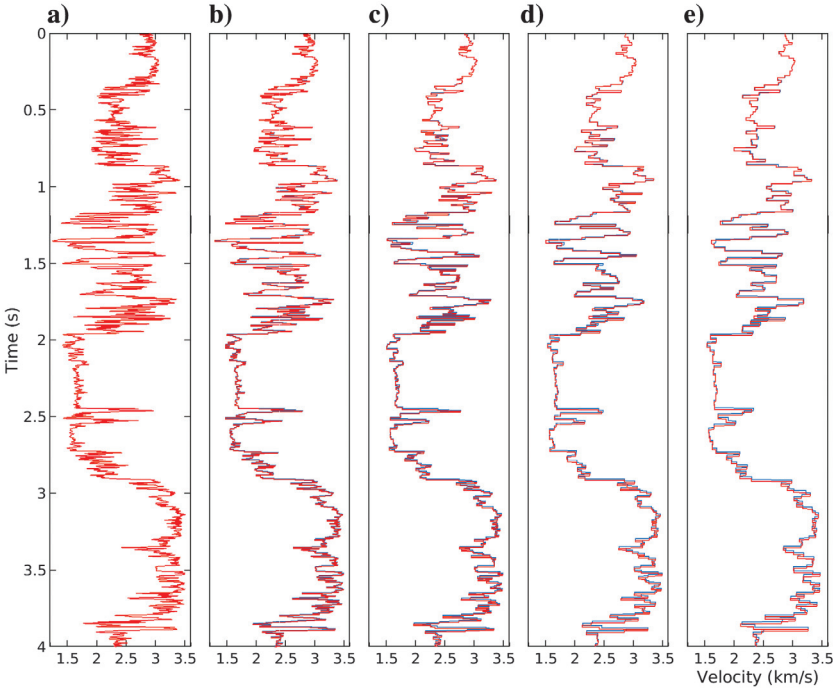

Figure 3. The sonic log with depth interval of 1 m has been upscaled up to the depth interval of 21 m with an increasing sample factor of 1 m. This figure shows selected upscaling logging data with depth interval of (a) 1 m, (b) 6 m, (c) 11 m, (d) 16 m, and (e) 21 m. In each plot, we compare the time-averaging upscaling result (the blue curve) with Backus averaging result (the red curve). There is only a small difference in upscaling results between the two methods.

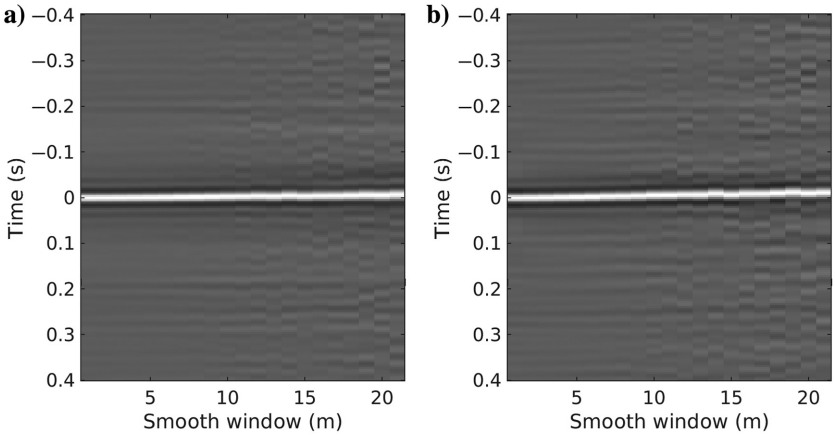

Figure 4. Comparisons of the impacts of the two model upscaling methods on the reflection data. The cross-coherence of primaries (internal multiples) generated by the time-averaging and Backus averaging upscaled velocity models with the same depth interval/upscaling window, length ranging from 1 to 21 m with an increment of 1 m, is aligned and displayed in (a and b), respectively. As seen, there is only one distinct spike-train event at zero-time lag, which indicates that primaries and internal multiples generated by the two different upscaling methods exhibit high similarities.

DOI:10.1190/geo2020-0874.1

ones. Subtle changes in primaries and significant changes in internal multiples are not as clear as the kurtosis curve of the cross-coherence results (Figure 7c).

SENSITIVITY OF THIN-LAYER SURFACE-RELATED MULTIPLES

To test the impact of fine layering on surface-related multiples, we add a free surface on top of the velocity model in Figure 2a. The surface-related multiples are obtained by the following steps: (1) compute the original synthetic traces $U(t)$ containing primaries and all orders of multiples, (2) set the reflection coefficient for the incident upgoing waves $r_u = 0$ for the surface layer, to obtain a new synthetic trace $U_1(t)$, and (3) subtract $U_1(t)$ from the original trace $U(t)$ to obtain a different trace $U_{\text{diff}}(t) = U(t) - U_1(t)$. The resulting trace $U_{\text{diff}}(t)$ contains all of the surface-related multiples that have experienced at least one downward reflection at the free surface.

We repeat the previous velocity model upscaling process and compare the impact of fine-scale variation in the velocity model on primaries and surface-related multiples. The primaries and surface-related multiples corresponding to the upscaled velocity models of the depth interval ranging from 1 to 21 m with an increment of 1 m are aligned and displayed in Figure 9a and 9b, respectively. As a reference, the first column shows the primaries and surface-related multiples generated by the original well log. Automatic gain control with 300 ms moving time window was applied on each trace to balance the amplitude difference. Similar to the previous tests, the influence of the fine layering on primaries is almost negligible (Figure 9a). However, differences are visible in the surface-related multiple panel shown in Figure 9b.

The comparisons of the kurtosis of the cross-coherence functions between the upscaled primaries/multiples and the original traces to quantify the differences are shown in Figure 10. Each column in Figure 10a corresponds to the cross-coherence result between the original primaries and the ones generated with upscaled velocity models. Figure 10b corresponds to the cross-coherence result between the original surface-related multiples and the ones generated with upscaled velocity models. Figure 10c shows the kurtosis of the primary and surface-related multiple cross-coherence results along with the upscaling window size. They exhibit the same trend as Figure 7c in general. The high kurtosis on the cross-coherence result of primaries (the blue curve in Figure 10c) indicates that the primaries are not sensitive to the fine-scale variation in the velocity model. However, the kurtosis of the cross-coherence result of surface-related multiples (the red curve in Figure 10c) drops dramatically as the size of the upscaled window increases.

As a comparison, we also compute the crosscorrelation of the primaries/surface-related multiples and their kurtosis. The resolution of crosscorrelation results of primaries (Figure 11a) and surface-related multiples (Figure 11b) is much lower than the cross-coherence results (Figure 10a and 10b). Moreover, changes on the kurtosis of primaries and surface-related multiples (Figure 11c) are not as clear as that of the cross-coherence results (Figure 10c).

DISCUSSION

Given the preceding analysis, we admit that short-period internal multiples help in transmitting energy through thin layers, and they are much more sensitive than primaries to the velocity changes. Considering the removal of internal multiples, we need to understand the physical reality that we are facing when removing internal

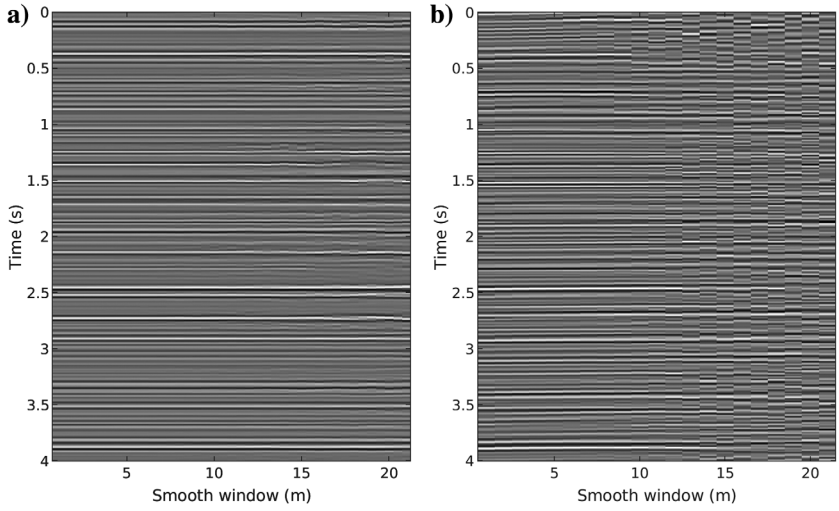

Figure 5. (a) The primaries and (b) internal multiples one-to-one correspond to the upscaled velocity models with depth interval of $1, 2, \ldots, 21$ m. Each column corresponds to a velocity model. The first columns of (a and b) are the primaries (Figure 2b) and internal multiples (Figure 2c) generated with the original thin-layer models.

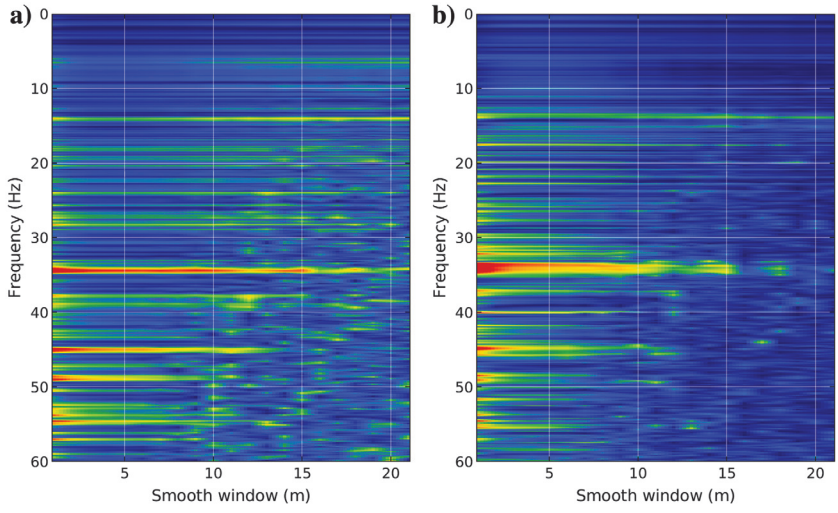

Figure 6. (a) The spectra of the primary impulse response (reflectivity). (b) The spectra of the impulse response of internal multiples. Each column corresponds to the upscaled velocity models with depth interval of $1, 2, \ldots, 21$ m.

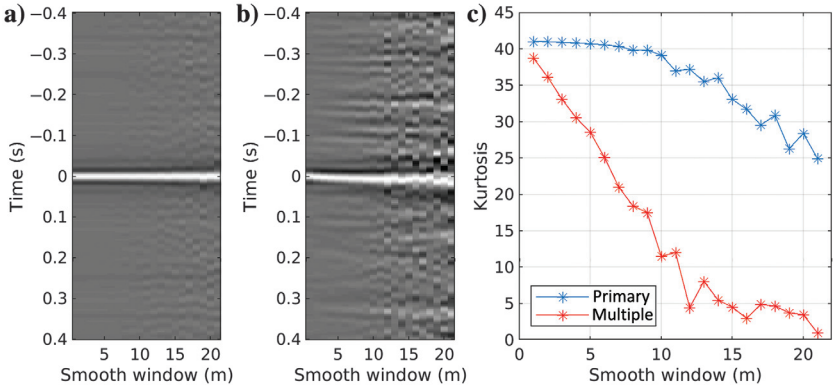

Figure 7. (a) The cross-coherence of the original primaries and the upscaled ones. (b) The cross-coherence of the original internal multiples and the upscaled ones. (c) The kurtosis curve of the cross-coherence results of primaries (blue) and internal multiples (red).

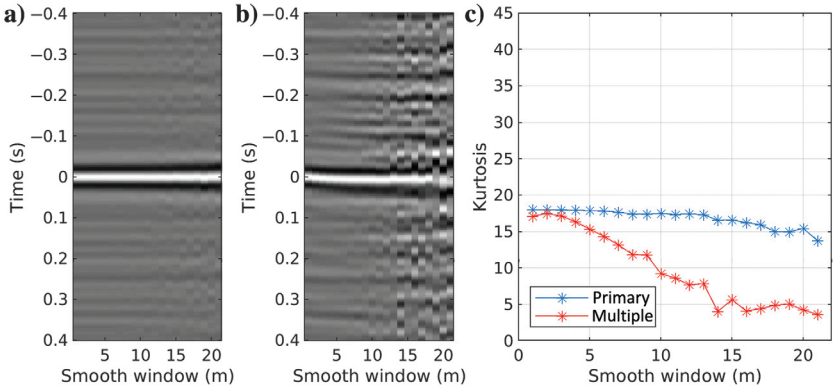

Figure 8. (a) The crosscorrelation of the original primaries and the upscaled ones. (b) The crosscorrelation of the original internal multiples and the upscaled ones. (c) The kurtosis curve of the crosscorrelation results of primaries (blue) and internal multiples (red).

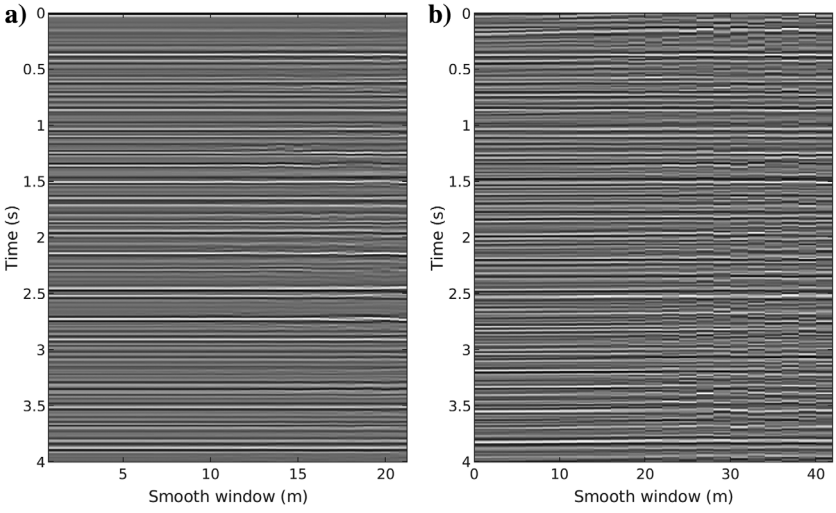

Figure 9. (a) The primaries and (b) surface-related multiples one-to-one correspond to the upscaled velocity models with depth interval of $1, 2, \ldots, 21$ m. Each column corresponds to a velocity model. A free surface is added on top of the velocity model.

multiples. The surface-related multiple removal process simulates the physical situation that the water has been filled to a level upward, whereas sources and receivers stay in the water at the same locations. In this situation, upcoming waves will not reach the surface and generate multiples within the registration time of the seismic data. For internal multiples, the situation is quite different. There is no physical model that exactly creates the same primary reflections only as the one we measure, without the internal multiples. Thus, the imaging algorithm would not create a physically realistic model from the measured primaries only. When we aim to remove internal multiples, especially the short-period ones for thin-layer models, we should simultaneously apply transmission correction to primaries to map them properly. Moreover, incorporating internal multiples properly in the imaging and inversion algorithms is the way forward from a physical point of view. In a manner similar to how the internal multiple removal is more complicated than the surface multiple removal, the imaging and inversion of internal multiples is an even larger challenge. Every subsurface grid point is a possible downward scatterer. We have shown that internal multiples are very sensitive on the fine layering. So how fine the velocity layer should be sampled to match the wavefield including primaries and short-period internal multiples is a problem to address. Because the kinematic sensitivity of internal multiples is related to the complicated travel path, how many orders of internal multiples should be considered properly for multiple imaging is another issue in reality. These problems are much more severe in inversion due to the high nonlinearity and the coupling effect of the fine layering on kinematic and amplitude information, especially for thin-layer velocity models (Liu et al., 2018, 2020a). Some attempts on imaging by using surface-related multiples and internal multiples can be found in Wang et al. (2014a, 2014b), Zheng et al. (2019), Wapenaar et al. (2014), Slob et al. (2014), Berkhout (2012, 2014), Davydenko and Verschuur (2014), and Berkhout and Verschuur (2016).

The velocity upscaling method used in this study is a time averaging of slowness within the given depth window for preserving kinematic information of primaries. It is well known that the vertical seismic resolution, which is one quarter of the dominant wavelength, is only suitable for primary reflections. The longer and more complicated travel path is the main reason that makes internal multiples more sensitive than primaries to the fine layering on velocity models. Liang et al. (2012) propose a reflector spectrum to quantitatively show the relative contribution of

DOI:10.1190/geo2020-0874.1

each individual reflector to all arrivals in a seismic trace. Their study confirms that, in a thin-layer velocity model, the observed primary often is the result of interference between a classic primary reflection and multiple reflections (O'Doherty and Anstey, 1971). Internal multiples originate from many reflectors. Thus, they cannot be eliminated by removing the effect of any single reflector or even a few major generators. Zhang et al. (2019) apply the data-driven T-MME to a four-layered synthetic example including a 30 m thin layer (the dominant wavelength of the data is 90 m). The result shows that the effect of limited bandwidth on thin-layer responses cannot be accounted for by the current scheme due to the fact that the thin-layer internal multiple is totally interfered with by the primary reflection.

Another topic that is worth mentioning is that the maximization of kurtosis of the cross-coherence between the observed and synthesized wavefields can be used as an objective function in seismic inversion to invert kinematic information for long-wavelength velocity components. Because the cross-coherence is much more sensitive to the similarity (or time alignment) of two traces than the crosscorrelation method, the combined use of kurtosis maximization and the cross-coherence function may have potential in reconstructing more details in the velocity model.

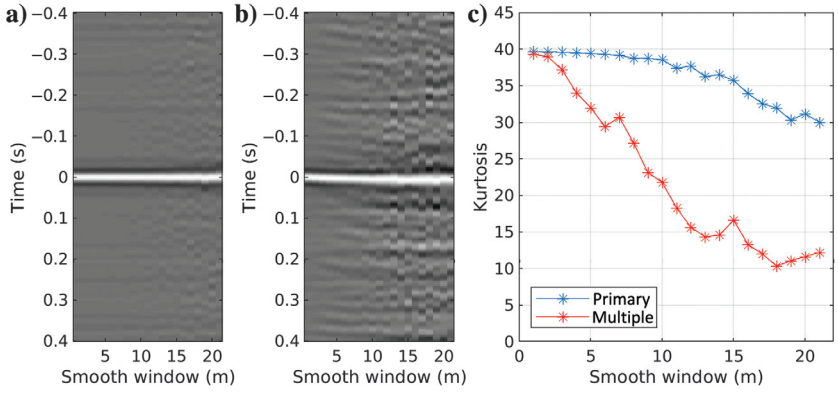

Figure 10. (a) The cross-coherence of the original primaries and the upscaled ones. (b) The cross-coherence of the original surface-related multiples and the upscaled ones. (c) The kurtosis curve of the cross-coherence results of primaries (blue) and surface-related multiples (red).

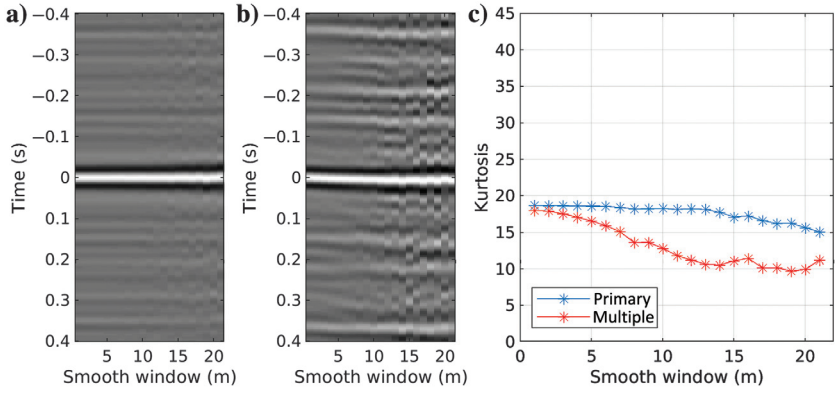

Figure 11. (a) The crosscorrelation of the original primaries and the upscaled ones. (b) The crosscorrelation of the original surface-related multiples and the upscaled ones. (c) The kurtosis curve of the crosscorrelation results of primaries (blue) and surface-related multiples (red).

CONCLUSION

We present a new approach to analyze the impact of fine-scale variations in the velocity model on primaries and multiples in the case of many thin layers. Cross-coherence is used to measure the similarity of the original primaries/multiples and the upscaled ones, and it shows much higher resolution than the crosscorrelation. The combined use of kurtosis and cross-coherence enables us to precisely quantify the impact of fine layering. Test results demonstrate that the internal multiples and surface-related multiples are much more sensitive than the primaries to fine-scale thickness variations in the velocity. As the thickness of each layer varies from 1 to 21 m, multiples change rapidly; however, primaries are almost the same. The high sensitivity of internal multiples on fine layering suggests that the detailed model information should be considered in model parameterization in the internal multiple prediction and elimination process. On the other hand, the high sensitivity of internal multiples on fine layering suggests that the detailed model information should be considered in model parameterization if the internal multiples are incorporated in imaging and full-waveform inversion. The parameterization scale should be designed based on the order of the internal multiples used in imaging or inversion.

DATA AND MATERIALS AVAILABILITY

Data associated with this research are confidential and cannot be released.

APPENDIX A

REFLECTION FROM A STACK OF UNIFORM LAYERS

We follow the reflectivity method in Kennett (2003) to construct the reflection response of a stratified medium to incident downgoing waves. Figure A-1 shows the N uniform layers with velocity model $v(z_i)$, where z_i is the depth of the ith reflector, $i = 1, \ldots, N$, the reflection and transmission coefficients at each interface for incident downgoing and upgoing waves are given by

$$r_d(z_i) = \frac{v(z_{i+1}) - v(z_i)}{v(z_{i+1}) + v(z_i)}, \tag{A-1}$$

$$t_d(z_i) = 1 - r_d(z_i), \tag{A-2}$$

$$r_u(z_i) = -r_d(z_i), \tag{A-3}$$

$$t_u(z_i) = 1 - r_u(z_i), \tag{A-4}$$

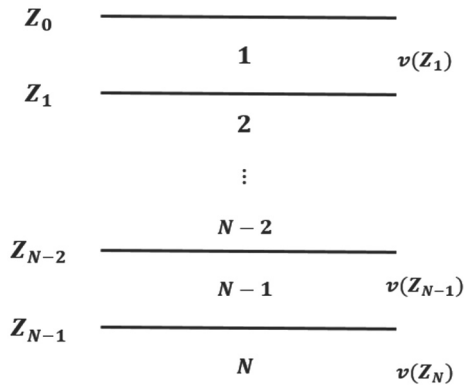

Figure A-1. An illustration of an N-layer velocity model.

where $r_d(z_i)$ and $t_d(z_i)$ are reflection and transmission coefficients for incident downgoing waves, respectively; $r_u(z_i)$ and $t_u(z_i)$ are reflection and transmission coefficients for incident upgoing waves, respectively; and $i = 1, \ldots, N$. Density is ignored for simplicity. We start at the bottom layer and calculate the reflection coefficient:

$$R_D(z_{N-1}^-) = r_d(z_{N-1}), \tag{A-5}$$

where z_{N-1}^- indicates the depth just above the layer z_{N-1}. Then, we add the phase terms and calculate the reflection just below the layer z_{N-2}:

$$R_D(z_{N-2}^+) = E_D^{N-1} R_D(z_{N-1}^-) E_U^{N-1}, \tag{A-6}$$

where z_{N-2}^+ indicates the depth just below the layer z_{N-2} and the phase term depends on the frequency ω and velocity:

$$E_D^{N-1} = E_U^{N-1} = e^{\frac{i\omega(z_{N-1}-z_{N-2})}{v(z_{N-1})}}. \tag{A-7}$$

After incorporating the interface at z_{N-2}, we bring the reflection to the upper side of the same layer:

$$R_D(z_{N-2}^-) = r_d(z_{N-2}) + \frac{t_d(z_{N-2}) R_D(z_{N-2}^+) t_u(z_{N-2})}{1 - r_u(z_{N-2}) R_D(z_{N-2}^+)}. \tag{A-8}$$

Note that the term $(1 - r_u(z_{N-2}) R_D(z_{N-2}^+))^{-1}$ in equation A-8 represents the cumulative effect of a sequence of internal reverberations, containing primaries and infinite orders of internal multiples. A Taylor series expansion of this term will separate the primary reflection, first-order multiple, and each high-order multiples explicitly.

Equations A-6–A-8 allow the construction of the reflection response recursively, a layer at a time for a stratified multilayer velocity model. As a result, a synthetic seismic trace is produced by the inverse Fourier transform of the products of different monochromatic impulse responses with a source wavelet.

REFERENCES

Abma, R., N. Kabir, K. H. Matson, S. A. Shaw, B. McLain, and S. Michell, 2002, Comparisons of adaptive subtraction techniques for multiple attenuation: 72nd Annual International Meeting, SEG, Expanded Abstracts, 2186–2189, doi: 10.1190/1.1817141.

Aki, K., 1957, Space and time spectra of stationary stochastic waves, with special reference to microtremors: Bulletin of the Earthquake Research Institute, University of Tokyo, **35**, 415–456.

Araújo, F. V., A. B. Weglein, P. M. Carvalho, and R. H. Stolt, 1994, Inverse scattering series for multiple attenuation: An example with surface and internal multiples: 64th Annual International Meeting, SEG, Expanded Abstracts, 1039–1041, doi: 10.1190/1.1822691.

Backus, G. E., 1962, Long-wave anisotropy produced by horizontal layering: Journal of Geophysical Research, **67**, 4427–4440, doi: 10.1029/JZ067i011p04427.

Bensen, G. D., M. H. Ritzwoller, M. P. Barmin, A. L. Levshin, F. Lin, M. P. Moschetti, N. M. Shapiro, and Y. Yang, 2007, Processing seismic ambient noise data to obtain reliable broad-band surface-wave dispersion measurements: Geophysical Journal International, **169**, 1239–1260, doi: 10.1111/j.1365-246X.2007.03374.x.

Berkhout, A. J., 2012, Combining full wavefield migration and full waveform inversion, a glance into the future of seismic imaging: Geophysics, **77**, no. 2, S43–S50, doi: 10.1190/geo2011-0148.1.

Berkhout, A. J., 2014, Review paper: An outlook on the future of seismic imaging — Part 2: Full-wavefield migration: Geophysical Prospecting, **62**, 931–949, doi: 10.1111/1365-2478.12154.

Berkhout, A. J., and D. J. Verschuur, 1997, Estimation of multiple scattering by iterative inversion — Part 1: Theoretical considerations: Geophysics, **62**, 1586–1595, doi: 10.1190/1.1444261.

Berkhout, A. J., and D. J. Verschuur, 2005, Removal of internal multiples with the common-focus-point (CFP) approach — Part 1: Explanation of the theory: Geophysics, **70**, no. 3, V45–V60, doi: 10.1190/1.1925753.

Berkhout, A. J., and D. J. Verschuur, 2016, Enriched seismic imaging by using multiple scattering: The Leading Edge, **35**, 128–133, doi: 10.1190/tle35020128.1.

Bruggerman, D. A. G., 1937, Calculation of the different physical constants of heterogenic substances III. The elastic constants of the quasi isotropic compounds of isotropic substances: Annalen der Physik, **29**, 160–178.

Davydenko, M., and D. J. Verschuur, 2014, Full wavefield migration in three dimensions: 84th Annual international Meeting, SEG, Expanded Abstracts, 3935–3940, doi: 10.1190/segam2014-1079.1.

Elison, P., M. S. Dukalski, K. de Vos, D. J. van Manen, and J. O. A. Robertsson, 2020, Data-driven control over short-period internal multiples in media with a horizontally layered overburden: Geophysical Journal International, **221**, 769–787, doi: 10.1093/gji/ggaa020.

Fu, Q., Y. Luo, P. G. Kelamis, S. Huo, G. Sindi, S. Hsu, and A. B. Weglein, 2010, The inverse scattering series approach toward the elimination of land internal multiples: 80th Annual International Meeting, SEG, Expanded Abstracts, 3456–3461, doi: 10.1190/1.3513567.

Kelamis, P. G., E. Verschuur, K. E. Erickson, R. L. Clark, and R. M. Burnstad, 2002, Data-driven internal multiple attenuation — Applications and issues on land data: 72nd Annual International Meeting, SEG, Expanded Abstracts, 2035–2038, doi: 10.1190/1.1817099.

Kelamis, P. G., W. Zhu, K. O. Al-Rufaii, and Y. Luo, 2006, Land multiple attenuation — The future is bright: 76th Annual International Meeting, SEG, Expanded Abstracts, 2699–2703, doi: 10.1190/1.2370082.

Kennett, B. L. N., 2003, The seismic wavefield: Introduction and theoretical development: Cambridge University Press.

Levy, S., and D. W. Oldenburg, 1987, Automatic phase correction of common-midpoint stacked data: Geophysics, **52**, 51–59, doi: 10.1190/1.1442240.

Liang, H., Y. Luo, P. G. Kelamis, and A. Weglein, 2012, Reflector spectrum for relating seismic arrivals to reflectors: Geophysics, **77**, no. 6, T239–T246, doi: 10.1190/geo2012-0162.1.

Lin, T. T., and F. J. Herrmann, 2013, Robust estimation of primaries by sparse inversion via one-norm minimization: Geophysics, **78**, no. 3, R133–R150, doi: 10.1190/geo2012-0097.1.

Liu, L., X. Duan, and Y. Luo, 2020a, Three-dimensional data-domain full traveltime inversion using a practical workflow of early-arrival selection: Geophysics, **85**, no. 4, U77–U86, doi: 10.1190/geo2019-0476.1.

Liu, L., Y. Wu, B. Guo, H. Song, and Y. Luo, 2018, Near-surface velocity estimation using source-domain full traveltime inversion and early-arrival waveform inversion: Geophysics, **83**, no. 4, R335–R344, doi: 10.1190/geo2017-0712.1.

Liu, Y., Y. Ma, and Y. Luo, 2020b, Source location with cross-coherence migration: Geophysics, **85**, no. 4, KS127–KS138, doi: 10.1190/geo2019-0311.1.

Löer, K., A. Curtis, and G. A. Meles, 2016, Relating source-receiver interferometry to an inverse-scattering series to derive a new method to estimate internal multiples: Geophysics, **81**, no. 3, Q27–Q40, doi: 10.1190/geo2015-0330.1.

Luo, Y., P. G. Kelamis, Q. Fu, S. Huo, G. Sindi, S. Hsu, and A. Weglein, 2011, Elimination of land internal multiples based on the inverse scattering series: The Leading Edge, **30**, 884–889, doi: 10.1190/1.3626496.

Luo, Y., W. Zhu, and P. G. Kelamis, 2007, Internal multiple reduction in inverse-data domain: 77th Annual International Meeting, SEG, Expanded Abstracts, 2485–2489, doi: 10.1190/1.2792983.
Matson, K., D. Corrigan, A. B. Weglein, C. Y. Young, and P. Carvalho, 1999, Inverse scattering internal multiple attenuation: Results from complex synthetic and field data examples: 69th Annual International Meeting, SEG, Expanded Abstracts, 1060–1063, doi: 10.1190/1.1820681.
Nakata, N., R. Snieder, T. Tsuji, K. Larner, and T. Matsuoka, 2011, Shear wave imaging from traffic noise using seismic interferometry by cross-coherence: Geophysics, **76**, no. 6, SA97–SA106, doi: 10.1190/geo2010-0188.1.
O'Doherty, R. F., and N. A. Anstey, 1971, Reflections on amplitudes: Geophysical Prospecting, **19**, 430–458, doi: 10.1111/j.1365-2478.1971.tb00610.x.
Oristaglio, M., 2013, SEAM phase II update: The Leading Edge, **32**, 606–608, doi: 10.1190/tle32060606.1.
Ramirez, A. C., and A. B. Weglein, 2008, Inverse scattering internal multiple elimination: Leading-order and higher-order closed forms: 78th Annual International Meeting, SEG, Expanded Abstracts, 2471–2475, doi: 10.1190/1.3063857.
Reinicke, C., M. Dukalski, and K. Wapnaar, 2021, Internal multiple elimination: Can we trust an acoustic approximation? Geophysics, **86**, no. 5, WC41–WC54, doi: 10.1190/GEO2020-0850.1.
Shen, X., T. Tonellot, Y. Luo, T. Keho, and R. Ley, 2012, A new waveform inversion workflow: Application to near-surface velocity estimation in Saudi Arabia: 82nd Annual International Meeting, SEG, Expanded Abstracts, 1–5, doi: 10.1190/segam2012-0024.1.
Slob, E., K. Wapenaar, F. Broggini, and R. Snieder, 2014, Seismic reflector imaging using internal multiples with Marchenko-type equations: Geophysics, **79**, no. 2, S63–S76, doi: 10.1190/geo2013-0095.1.
Staring, M., M. Dukalski, M. Belonosov, R. Baardman, J. Yoo, R. Hegge, R. van Borselen, and K. Wapenaar, 2021, Robust estimation of primaries by sparse inversion and Marchenko equation-based workflow for multiple suppression in the case of a shallow water layer and a complex overburden: A 2D case study in the Arabian Gulf: Geophysics, **86**, no. 2, Q15–Q25, doi: 10.1190/geo2020-0204.1.
Tiwary, D. K., I. Bayuk, A. Vikhorev, and E. Chesnokov, 2009, Comparison of seismic upscaling methods: From sonic to seismic: Geophysics, **74**, no. 2, WA3–WA14, doi: 10.1190/1.3054144.
Trad, D., T. Ulrych, and M. D. Sacchi, 2003, Latest views of the sparse Radon transform: Geophysics, **68**, 255–261, doi: 10.1190/1.1543224.
Van der Neut, J., and K. Wapenaar, 2016, Adaptive overburden elimination with the multidimensional Marchenko equation: Geophysics, **81**, no. 5, T265–T284, doi: 10.1190/geo2016-0024.1.
Van Groenestijn, G. J. A., and D. J. Verschuur, 2009, Estimating primaries by sparse inversion and application to near-offset data reconstruction: Geophysics, **74**, no. 3, A23–A28, doi: 10.1190/1.3111115.
Verschuur, D. J., and A. J. Berkhout, 2015, From removing to using multiples in closed-loop imaging: The Leading Edge, **34**, 744–759, doi: 10.1190/tle34070744.1.
Wang, Y., X. Chang, and H. Hu, 2014a, Simultaneous reverse time migration of primaries and free-surface related multiples without multiple prediction: Geophysics, **79**, no. 1, S1–S9, doi: 10.1190/geo2012-0450.1.
Wang, Y., Y. Zheng, L. Zhang, X. Chang, and Z. Yao, 2014b, Reverse time migration of multiples: Eliminating migration artifacts in angle domain common image gathers: Geophysics, **79**, no. 6, S263–S270, doi: 10.1190/geo2013-0441.1.
Wapenaar, K., J. Thorbecke, J. van der Neut, F. Broggini, E. Slob, and R. Snieder, 2014, Marchenko imaging: Geophysics, **79**, no. 3, WA39–WA57, doi: 10.1190/geo2013-0302.1.
Weglein, A. B., 2016, Multiples: Signal or noise? Geophysics, **81**, no. 4, V283–V301, doi: 10.1190/geo2014-0486.1.
Weglein, A. B., F. A. Gasparotto, P. M. Carvalho, and R. H. Stolt, 1997, An inverse scattering series method for attenuating multiples in seismic reflection data: Geophysics, **62**, 1975–1989, doi: 10.1190/1.1444298.
Ypma, F. H. C., and D. J. Verschuur, 2013, Estimating primaries by sparse inversion, a generalized approach: Geophysical Prospecting, **61**, 94–108.
Zhang, L., and E. Slob, 2019, Free-surface and internal multiple elimination in one step without adaptive subtraction: Geophysics, **84**, no. 1, A7–A11, doi: 10.1190/geo2018-0548.1.
Zhang, L., and E. Slob, 2020, A field data example of Marchenko multiple elimination: Geophysics, **85**, no. 2, S65–S70, doi: 10.1190/geo2019-0327.1.
Zhang, L., and M. Staring, 2018, Marchenko scheme based internal multiple reflection elimination in acoustic wavefield: Journal of Applied Geophysics, **159**, 429–433, doi: 10.1016/j.jappgeo.2018.09.024.
Zhang, L., J. Thorbecke, K. Wapenaar, and E. Slob, 2019, Transmission compensated primary reflection retrieval in data domain and consequences for imaging: Geophysics, **84**, no. 4, Q27–Q36, doi: 10.1190/geo2018-0340.1.
Zheng, Y., Y. Wang, and X. Chang, 2019, Least-squares data-to-data migration: An approach for migrating free-surface-related multiples: Geophysics, **84**, no. 2, S83–S94, doi: 10.1190/geo2018-0080.1.

Biographies and photographs of the authors are not available.